Using Routinely Available Information to Estimate Tropical Cyclone Wind Structure

JOHN A. KNAFF

NOAA/Center for Satellite Applications and Research, Fort Collins, Colorado

CHRISTOPHER J. SLOCUM

Department of Atmospheric Science, Colorado State University, Fort Collins, Colorado

KATE D. MUSGRAVE

Cooperative Institute for Research in the Atmosphere, Colorado State University, Fort Collins, Colorado

CHARLES R. SAMPSON

Naval Research Laboratory, Monterey, California

BRIAN R. STRAHL

Joint Typhoon Warning Center, Pearl Harbor, Hawaii

(Manuscript received 28 July 2015, in final form 14 December 2015)

ABSTRACT

A relatively simple method to estimate tropical cyclone (TC) wind radii from routinely available information including storm data (location, motion, and intensity) and TC size is introduced. The method is based on a combination of techniques presented in previous works and makes an assumption that TCs are largely symmetric and that asymmetries are based solely on storm motion and location. The method was applied to TC size estimates from two sources: infrared satellite imagery and global model analyses. The validation shows that the methodology is comparable with other objective methods based on the error statistics. The technique has a variety of practical research and operational applications, some of which are also discussed.

1. Introduction

Global tropical cyclone (TC) warning centers routinely estimate the maximum radial extent of significant wind speed thresholds (e.g., the radial extent of 34-kt wind speed) as part of their TC advisory and warning process. These estimates are typically referred to collectively as wind radii. At the National Hurricane Center (NHC), the Central Pacific Hurricane Center (CPHC), and the Joint Typhoon Warning Center (JTWC), these wind radii come in the form of the maximum radial extent of 34-, 50-, and 64-kt (kt, where 1 kt = 0.514 m s^{-1}) winds in geographic quadrants (i.e., in the northeast, southeast, southwest, and northwest directions).[1] These distances are reported in units of nautical miles (n mi, where 1 n mi = 1.85 km). (For this reason, the operational units of kt and n mi are used exclusively hereafter.) NHC and CPHC have been routinely conducting postseason reanalysis or best tracking of these wind radii since 2004, so this study will make use of this quality-controlled dataset.

Wind radii estimates made by operational centers are based on subjective analyses of the available information.

Corresponding author address: John Knaff, NOAA/RAMMB, CIRA/CSU, Campus Delivery 1375, Fort Collins, CO 80523-1365. E-mail: john.knaff@noaa.gov

[1] Descriptions of the NHC's Tropical Cyclone Forecast/Advisory and graphical Tropical Cyclone Wind Field can be found online at http://www.nhc.noaa.gov/aboutnhcprod.shtml#TCM and http://www.nhc.noaa.gov/aboutnhcgraphics.shtml?#INITIALWIND, respectively.

DOI: 10.1175/MWR-D-15-0267.1

In situ observations such as surface reports and buoy observations can provide high-quality ground truth, but these observations are not routinely available. Aircraft reconnaissance can also provide detailed spatial distribution of the low-level or surface winds, but these are rarely available outside the North Atlantic region. The dearth of in situ observations makes routine operational wind radii estimation heavily dependent upon satellite observations and techniques. Satellite observations include cloud/feature-tracked winds (Holmlund et al. 2001; Velden et al. 2005) and scatterometry (Jones et al. 1975). In addition to these remotely sensed wind vectors, there are several operational tools specifically designed to estimate TC vortex structure. These include techniques that estimate wind radii directly from microwave sounders (Demuth et al. 2004, 2006) and methods that estimate the flight-level winds using information derived from infrared (IR) satellite imagery, TC intensity, and TC motion (Mueller et al. 2006; Kossin et al. 2007; Knaff et al. 2015). These IR-based flight-level wind estimate techniques employ different methods and are trained on aircraft analyses of flight-level observations. Another method, which is operationally available, combines information of multiple satellite-based techniques including scatterometry, cloud/feature-tracked winds, winds based on microwave sounders, and the Mueller et al. (2006) IR method as described in Knaff et al. (2011). Each of these methods and observations has its own weaknesses. As a result, errors in operational (and best tracked) wind radii estimates can at times be as large as 25%–40% of the radii themselves (see Knaff and Harper 2010; Knaff and Sampson 2015). One could take the pessimist view that the best-tracked wind radii are of little worth. That is not our view. Here we presume that best-tracked wind radii estimates produced by operational centers are of the highest quality possible and thus are useful for many applications.

The production of quality wind radii is important to operations for a number of reasons beyond the obvious specification of TC vortex structure. The primary purpose of wind radii is to provide quantitative estimates of the TC wind structure for the production of effective warnings of on-station and on-ship gale-force (34 kt), damaging (50 kt), and destructive winds (64 kt) winds. Wind radii provide initial conditions for a number of applications such as wind speed probabilities (DeMaria et al. 2009, 2013), TC conditions of readiness (Sampson et al. 2012) and wave forecasting (Sampson et al. 2010), and also for numerical models like the GFDL (Bender et al. 2007) and HWRF (Tallapragada et al. 2014). Specifying the correct initial TC surface wind structure also appears to improve hurricane model track and intensity performance (Bender et al. 2015). In addition, the extent of the primary vortex has been shown to be important for vortex resiliency (Reasor et al. 2004), the evolution of the inner-core structure (Xu and Wang 2010), the response of winds to convective heating (Musgrave et al. 2012), the potential for secondary eyewall formation (Rozoff et al. 2012), future intensification rates (Xu and Wang 2015), etc. As TCs age and move poleward, their wind radii tend to expand (Ooyama 1969; Merrill 1984; Chan and Chan 2014); however, this interpretation is probably too simplistic since TC intensity and inertial stability also play fundamental roles in wind radii changes (Shapiro and Willoughby 1982; Schubert and Hack 1982; Smith et al. 2011). The bottom line is that careful monitoring of TC structure changes is warranted.

Asymmetries in wind radii are important to operations as they affect the distribution of high seas associated with TCs (Lazarus et al. 2013; Sampson et al. 2010), storm surge and inundation (Probst and Franchello 2012), and other risks. Asymmetries in the primary vortex are the result of motion and convective asymmetries. The latter is often related to vertical wind shear. In this work, only the motion-induced asymmetries are explicitly addressed.

There are several approaches that could be taken to generate two-dimensional continuous wind fields from wind radii, and the authors have chosen a modified Rankine vortex (MRV) for use in this study because of its simplicity and proven stability in the operational setting. The form of the MRV used here follows DeMaria et al. (2009), but each wind radii wind speed threshold is treated separately, a climatological radius of maximum wind (R_m) is used [described in Knaff et al. (2015)], and the azimuthal wavenumber-1 asymmetries are determined by storm motion and latitude following Knaff et al. (2007). A full description of the MRV methodology is provided in section 2. We feel this is a good assumption for tropical cyclone–like vortices in low to moderate wind shear environments since we are treating each wind threshold separately and the motion-related surface wind asymmetries tend to dominate in these situations (Uhlhorn et al. 2014). We recognize that the wind shear vector plays a role in the location of azimuthal wavenumber-1 (downshear left), as shown in Uhlhorn et al. (2014). We also are aware that such assumptions are weaker for extratropical cyclones, as discussed in Loridan et al. (2014), and moderately to strongly sheared cyclones where large downshear convective asymmetries [i.e., as shown in Bender (1997) and Frank and Ritchie (2001)] are likely contributing to surface wind enhancements.

Wind radii are also related to the TC vortex size that is typically defined by the radius of zero tangential wind. The initial TC size is also important as it determines to first order the future size (Lee et al. 2010; Knaff et al. 2014, hereafter KLM). While storm sizes tend to remain fairly constant (e.g., Chavas and Emanuel 2010; KLM), the wind radii often grow in response to influxes of angular momentum (Chan and Chan 2013). To construct a 30-yr record of TC size, KLM introduced a satellite-based method that related the azimuthally averaged 850-hPa tangential winds (from model analyses) to the radial distribution of azimuthally averaged infrared ($\sim$11 μm) brightness temperatures. KLM also discussed briefly how the TC size parameter, R5, along with intensity could be used to estimate the symmetric 34-kt wind radii. While TC size, as defined here, is dynamically and scientifically important, it is a rather difficult quantity to measure directly and not operationally relevant.

To make the satellite-based method introduced in KLM more operationally relevant, this paper will expand on the idea of using satellite-based TC size information (i.e., R5) along with current intensity to construct realistic wind radii estimates. The following sections will discuss the datasets used, the details of the construction of this methodology, the validation of this technique, and some future directions.

2. Data and methods

a. Necessary information

In this paper, the term ''routinely available'' refers to information that is available at most operational TC forecast centers in real time. These would include TC-specific information about the intensity, location, and motion of a storm as well as digital geostationary satellite data and model analyses. A combination of TC best tracks, model analyses, and satellite imagery archives allow these data to be available in a research setting. Figure 1 provides a flowchart for the procedures presented in this section.

For the method introduced here, routine information about the intensity, motion, and size is all that is needed to estimate wind radii. Intensity and motion are most often estimated from satellite information, but can also be derived from aircraft reconnaissance–based information when available. Locating the TC center is part of the intensity estimation process and is also used to determine the TC motion. Satellite-based intensity estimates come from several methods including subjective (Dvorak 1984; Velden et al. 2006) and objective Dvorak techniques (Olander and Velden 2007), microwave

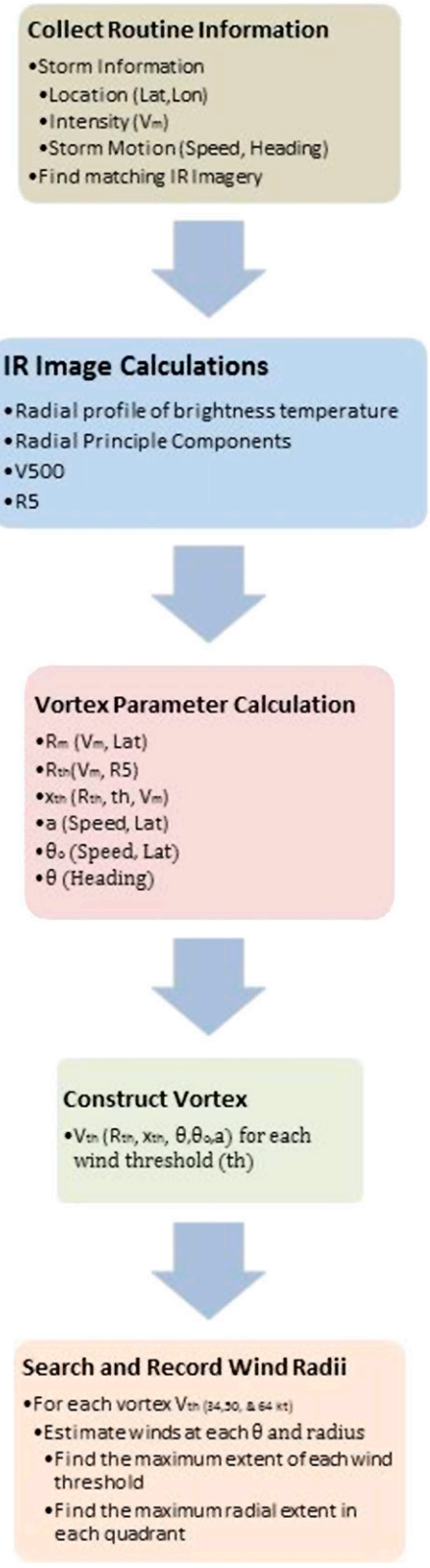

FIG. 1. The steps taken to estimate 34-, 50-, and 64-kt wind radii using the method discussed in this paper. Principle components based on the radial profiles of brightness temperature are used to estimate V500 as described in KLM as part of the IR image calculations.

methods (Demuth et al. 2006; Herndon and Velden 2004), and consensus methods (Herndon et al. 2012). The radius of maximum wind R_m, an important vortex parameter, can be estimated from satellite when an eye exists in the IR (e.g., Kossin et al. 2007) and from passive microwave data, but in many instances, a ''reasonable'' estimate of R_m is provided.[2] Size for this study will be derived from the azimuthally averaged tangential wind at 500 km (V500) first presented in Knaff and Zehr (2007). This metric can be estimated from global model analyses, via satellite as discussed in KLM, or even by stochastically sampling historical distributions. V500 is then used to estimate a size parameter, R5, as described in KLM. The units of R5 are degrees latitude, and

$$\mathrm{R5} = \overline{\mathrm{R5}} + \alpha\left(\frac{\mathrm{V500} - \mathrm{V500c}}{\mathrm{V500c} - \mathrm{V1000c}}\right), \tag{1}$$

where $\alpha = 4.5°$ latitude, $\overline{\mathrm{R5}} = 8.6°$ latitude, V500c = 5.05 m s^{-1}, and V1000c = 2.23 m s^{-1}, and the azimuthally averaged tangential wind at 500 and 1000 km are defined as V500 and V1000, respectively. The climatological values V500c and V1000c were calculated from information in the developmental data of the Statistical Hurricane Intensity Predictions Scheme (SHIPS; RAMMB/CIRA 2015).[3] More complete details are described in KLM. It is worth noting, however, that intensity and motion can come from any track realization observed or simulated.

For the remainder of this study R_m is estimated by the climatological relationship between R_m and a combination of intensity V_m and latitude γ as described in Knaff et al. (2015):

$$R_m = 218.3784 - 1.2014V_m + \left(\frac{V_m}{10.9844}\right)^2 - \left(\frac{V_m}{35.3052}\right)^3 - 145.5090\cos\gamma, \tag{2}$$

where R_m has units of n mi, V_m has units of kt, and latitude γ has units of degrees. This relationship explains approximately 17%–33% of the variance depending on validation sample (Knaff et al. 2015) and thus is reasonable and stable estimate.

TABLE 1. Statistics for the multiple regression equations relating intensity and R5 to the azimuthally averaged 34-, 50-, and 64-kt wind radii ($\overline{\mathrm{R34}}$, $\overline{\mathrm{R50}}$, and $\overline{\mathrm{R64}}$) are listed. The amount of variance explained (R^2), the intercept, and the regression coefficients are provided. Units for these statistics are n mi, where 1 n mi = 1.85 km.

R_{th}	R^2	Intercept	Intensity coef	R5 coef
$\overline{\mathrm{R34}}$	0.41	−58.5	0.71	9.26
$\overline{\mathrm{R50}}$	0.45	−54.1	0.50	5.90
$\overline{\mathrm{R64}}$	0.46	−32.9	0.29	3.30

b. Tropical cyclone vortex methodology

As discussed in the introduction, the TC vortex is parameterized using an MRV where the azimuthally averaged wind field is a function of the intensity V_m, radius r, and a shape parameter x. The MRV produces a peaked wind maximum, which is desirable for this application and quite different from many other common vortex parameterizations. To account for asymmetries as a function of azimuth θ, parameters θ_o, the degree of rotation of the asymmetry from the direction 90° to the right of the storm motion vector, and the variable a defined as the magnitude of the asymmetry are also required. As in DeMaria et al. (2009), the variation of wind speed as a function of r and θ is defined as

$$V(r,\theta) = (V_m - a)\left(\frac{r}{R_m}\right) + a\cos(\theta - \theta_o), \quad r < R_m \tag{3a}$$

$$V(r,\theta) = (V_m - a)\left(\frac{R_m}{r}\right)^x + a\cos(\theta - \theta_o), \quad r \geq R_m. \tag{3b}$$

The first parameters calculated are the azimuthally averaged 34-, 50-, and 64-kt wind radii (i.e., $\overline{\mathrm{R34}}$, $\overline{\mathrm{R50}}$, or $\overline{\mathrm{R64}}$, respectively) that are based on multiple regression using R5 and V_m. The multiple regressions relate the observed nonzero azimuthally averaged 34-, 50-, and 64-kt wind radii from the Atlantic and east Pacific (1995–2012) with corresponding V_m from the best tracks and 6-hourly estimates of R5 calculated from using the Cooperative Institute for Research in the Atmosphere (CIRA) Regional and Mesoscale Meteorology Branch (RAMMB) IR TC image archive (see Mueller et al. 2006; KLM). The regression coefficients for the R_{th} (where th = 34, 50, or 64 kt) relationships, which were developed for this application, are listed in Table 1. The use of different decay rates partially overcomes some of the undesirable biases

[2] The variable R_m is provided as part of the 6-hourly Combined Automated Request Query (CARQ) line in the Automated Tropical Cyclone Forecast (ATCF; Sampson and Schrader 2000) databases. These estimates are provided solely for model initialization and are often simply a reasonable estimate that will not negatively affect numerical guidance. The resulting R_m values are not best tracked following the season, but sometimes appear in the best-track files.

[3] The parameter values used to calculate R5 are those provided in KLM and not those in the corrigendum of that work.

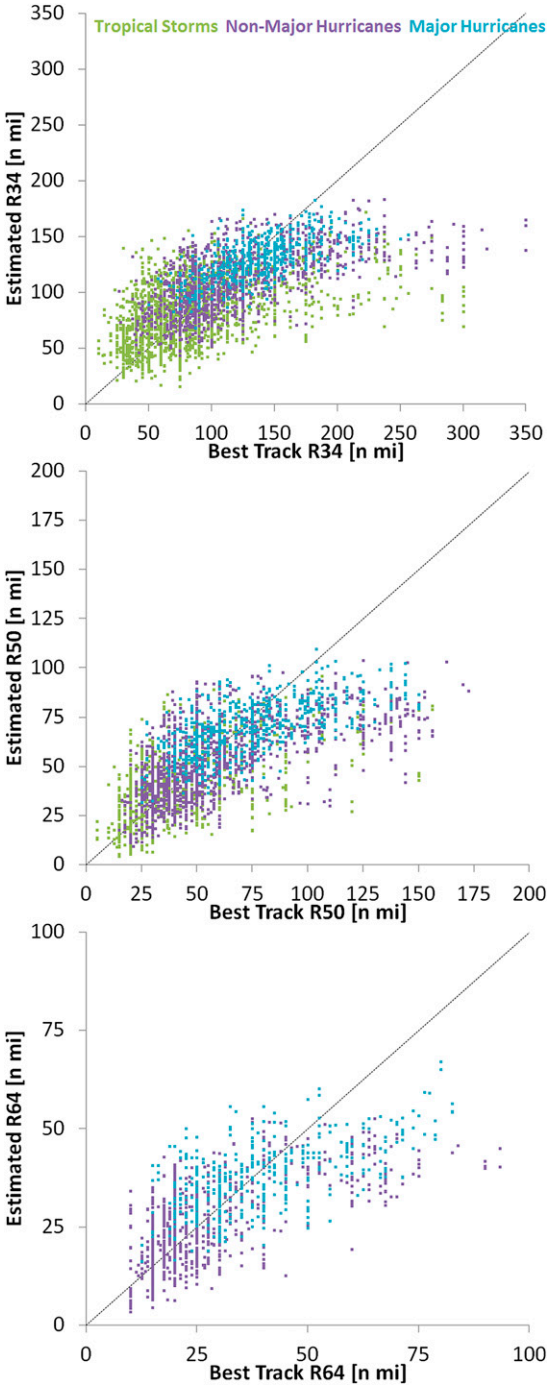

FIG. 2. Scatter diagrams showing the dependent sample of estimated (top) $\overline{\text{R34}}$, (middle) $\overline{\text{R50}}$, and (bottom) $\overline{\text{R64}}$ versus observed values. The colors of the points indicate tropical storm intensity (green), nonmajor hurricane intensity (purple), and major hurricane intensity cases (light blue).

that occur in wind profiles produced by MRV that uses a single decay rate. Figure 2 shows the corresponding scatterplots associated with these fits as a function of intensity. The scatter show how these relationships saturate for the largest observed cases, which may result in some biases, but also provide stability to the estimates. This saturation may, however, be expected as a recent study suggests that TC 34-kt wind radii generally increase during intensification until the storm reaches an intensity of approximately 100 kt and/or 34-kt wind radii of 150 n mi (Wu et al. 2015).

In most cases, using a climatological R_m is unavoidable as the R_m is difficult to estimate due to the lack of in situ observations, particularly for storms that do not have eye features, and weaker systems. Because the estimate of azimuthally averaged wind radii can for a few cases be less than the climatological R_m, the following strategy was adopted. The azimuthally averaged wind radius, regardless of threshold, is set to the maximum of the predicted azimuthally averaged wind radii or 1.25 times the climatological R_m. The result of this strategy is a possible overestimation of the wind radius associated with the wind threshold closest to the R_m. Cases like this occur less than 3% of the time. With the exception of these special cases that typically occur when the storm intensity is close to the wind radii threshold, there is little effect on the outer wind radii since $\overline{\text{R34}}$, $\overline{\text{R50}}$, and $\overline{\text{R64}}$ are estimated separately.

The estimation of the shape parameter (x_{th}) for each wind speed threshold is calculated from the decay of the azimuthally averaged wind radii from R_m, where the wind speed is equal to the V_m. This is accomplished by using Eq. (4), where th represents the wind speed threshold and R_{th} is the azimuthally average wind radii associated with that threshold (i.e., $\overline{\text{R34}}$, $\overline{\text{R50}}$, and $\overline{\text{R64}}$). Note that for this algorithm x_{th} are also constrained to fall between 0.1 and 1.0:

$$x_{\text{th}} = \log[(\text{th}/V_m)/(R_m/R_{\text{th}})]. \quad (4)$$

To calculate the magnitude a and storm-motion-oriented rotation θ_o of the asymmetric part of the parameterized vortex, the climatological relationships developed for the North Atlantic version of the wind radii climatology and persistence model [i.e., Table 1 of Knaff et al. (2007)] are used. In this formulation,

$$a = 1.06 + 0.28c - 0.0026c^2 - 0.08(\gamma - 25) \quad \text{and} \quad (5)$$

$$\theta_o = 17.0 + 0.08(\gamma - 25) - 1.05c, \quad (6)$$

where c is the storm speed with units of knots, and γ is latitude in degrees poleward. The same values of a and θ_o are used for each wind speed threshold.

Using the parameters V_m, R_m, a, θ_o, and θ (i.e., perpendicular to the provided motion vector), x_{34}, x_{50}, and x_{64}, and the MRV equations in Eqs. (3a) and (3b),

complete vortices for each wind threshold (i.e., V_{34}, V_{50}, and V_{64}) are constructed. The value of V_m determines which vortex equations are used. For instance, if V_m is 55 kt only V_{34} and V_{50} are constructed. By searching through each azimuth, the maximum extent of each wind threshold in each quadrant can be found.

This vortex methodology results in wind radii estimates that are most valid for a TC vortex moving through the tropical or subtropical atmosphere where horizontal pressure gradients are relatively weak and implicitly assumes a degree of vortex symmetry. Experience also suggests that the MRV method, if properly calibrated, will produce stable estimates and provide relatively good validation statistics when compared to the best track or extended best track (e.g., Demuth et al. 2006; Knaff et al. 2007). Again, to aid the reader, a flowchart describing the procedures used here is provided in Fig. 1.

3. Validation of concept

To validate this methodology, we use a perfect prognostic method or perfect prog approach (Kalnay 2003), where the ''perfect'' estimates of storm intensity, location, and motion are provided from the final best track data. The TC size can be based on IR imagery, model analyses, or by other means. The value of R_m is again provided by climatology. The intensity, location, and motion are interpolated to the image time for the calculations. If the best track wind radii are also considered perfect, the only remaining and unaccountable errors presumably are those associated with the TC size estimates, and the R_m.

This perfect prog approach is applied using two options: 1) R5 derived from IR satellite images, and/or 2) using R5 values derived from the Global Forecast System (GFS) model analyses used for the development of the SHIPS (DeMaria et al. 2005; RAMMB/CIRA 2015). Satellite-based R5 are based on azimuthally averaged IR brightness temperatures and as such are most valid for TCs that are convectively active and have generally symmetric IR appearances [i.e., are evolved past the formative stage, not moving faster than about 8 m s^{-1} or 16 kt, not undergoing extratropical transition, and under moderate to weak vertical wind shear (i.e., <16 kt)]. The analysis-based R5 are calculated by averaging 8 points surrounding the storm location interpolated from the 1° GFS analyzed to obtain V500 that have made use of evolving operational gridpoint statistical interpolation (Developmental Testbed Center 2015) data assimilation (DA) process. It is recognized that both the DA process and the interpolation from analysis grid points may act to smooth the estimation of V500 and R5. Also, these calculations may be influenced by large asymmetries in V500. Table 2 shows the verification of these estimates versus the NHC best track data for 2004–13, noting that the verification is not homogeneous and contains Atlantic and east Pacific cases. Since the best track wind radii are used through 2010 for algorithm development, these results are further stratified into dependent (2004–10) and independent (2011–13) subsets.

Table 2 shows that the performance of the IR-derived wind radii is superior to those estimated directly from numerical analyses with analysis-based wind radii being generally high biased. This finding is not surprising since the wind radii algorithm was trained with R5 estimates made from IR imagery and numerical analyses may have difficulty resolving intense and small TC vortices.

TABLE 2. Mean absolute errors (MAE) and bias statistics for IR-derived and model analysis-derived wind radii estimates are shown for the dependent years (2004–10) and the independent years (2011–13). The number of cases for R34, R50, and R64, respectively, is provided by N at the top of each sample. Statistics are shown from individual directional quadrants and from the nonzero average of the individual quadrant wind radii or ALL as explained in the text, which provides an estimate of the overall size errors. Units for these statistics are n mi, where 1 n mi = 1.85 km.

	IR-derived R5				
	NE	SE	SW	NW	ALL
Dependent results (2004–10), N = 13 066, N = 8214, and N = 5020					
R34 MAE	35	31	31	36	29
R34 bias	−4	−6	7	7	−5
R50 MAE	20	19	19	20	17
R50 bias	−3	−1	7	3	−2
R64 MAE	13	12	11	13	11
R64 bias	−1	0	1	1	−1
Independent results (2011–13), N = 6296, N = 3500, and N = 1762					
R34 MAE	44	37	36	41	37
R34 bias	−13	−7	15	5	−12
R50 MAE	21	21	23	23	20
R50 bias	−1	3	12	7	−3
R64 MAE	13	13	13	14	12
R64 bias	3	5	5	4	0
	Analysis-derived R5				
	NE	SE	SW	NW	ALL
Results (2004–10), N = 2958, N = 2143, and N = 1338					
R34 MAE	46	38	31	43	35
R34 bias	23	16	13	26	16
R50 MAE	25	23	19	23	21
R50 bias	9	10	10	11	8
R64 MAE	19	15	11	16	14
R64 bias	9	6	−3	5	8
Results (2011–13), N = 1371, N = 920, and N = 478					
R34 MAE	41	36	30	39	31
R34 bias	11	12	17	18	8
R50 MAE	25	24	19	23	21
R50 bias	8	11	11	10	5
R64 MAE	17	16	10	15	13
R64 bias	9	9	0	0	6

TABLE 3. The ranges of latitude, translation speed, and radius of outermost isobar (ROCI) used to composite errors and bias statistics are listed.

Intensity (kt)		
Tropical storm (TS)	Nonmajor hurricane (NMH)	Major hurricane
≥34.0 and <65.0	≥65.0 and <96.0	≥96.0
Latitude (°)		
Low latitude <25		High latitude ≥25
Translation Speed (kt)		
Slow <6.0	Avg ≥6.0 and <14.0	Fast ≥14.0
ROCI (n mi)		
Small <165	Avg ≥165 and <270	Large ≥270

The strong serial correlation (~0.80 for R34) of wind radii errors in all quadrants makes the 95% confidence intervals relatively large (about 2–3 n mi) (Wilks 2006), but these differences are still statistically significant at the 95% level.

The independent IR-derived wind radii have poorer performance when compared to the larger dependent results than would be anticipated. These differences in performance are not statistically significant because confidence intervals are ~5–6 n mi for R34, but possible reasons for these differences are still worth discussing. The mean intensities of the dependent cases are 64, 77, and 91 kt, for R34, R50, and R64, respectively, whereas the intensities of the independent cases are 58, 70, and 83 kt, again, respectively. The weaker TCs are generally more asymmetric, making wind radii more difficult to estimate (Knaff and Sampson 2015). Another potential reason for the different behavior is the baroclinic nature of some of the TCs that occurred during 2011–13. For instance, the IR-derived method performed very poorly for the latter half of Hurricane Sandy's (2012) best track. It is interesting that a similar degradation of analysis-derived wind radii does not occur; suggesting that the model analyses that are unaffected by the poor convective signature, may provide superior estimates in cases like Sandy. However, the inclusion of influences of the environment on the analysis-derived R5 estimates

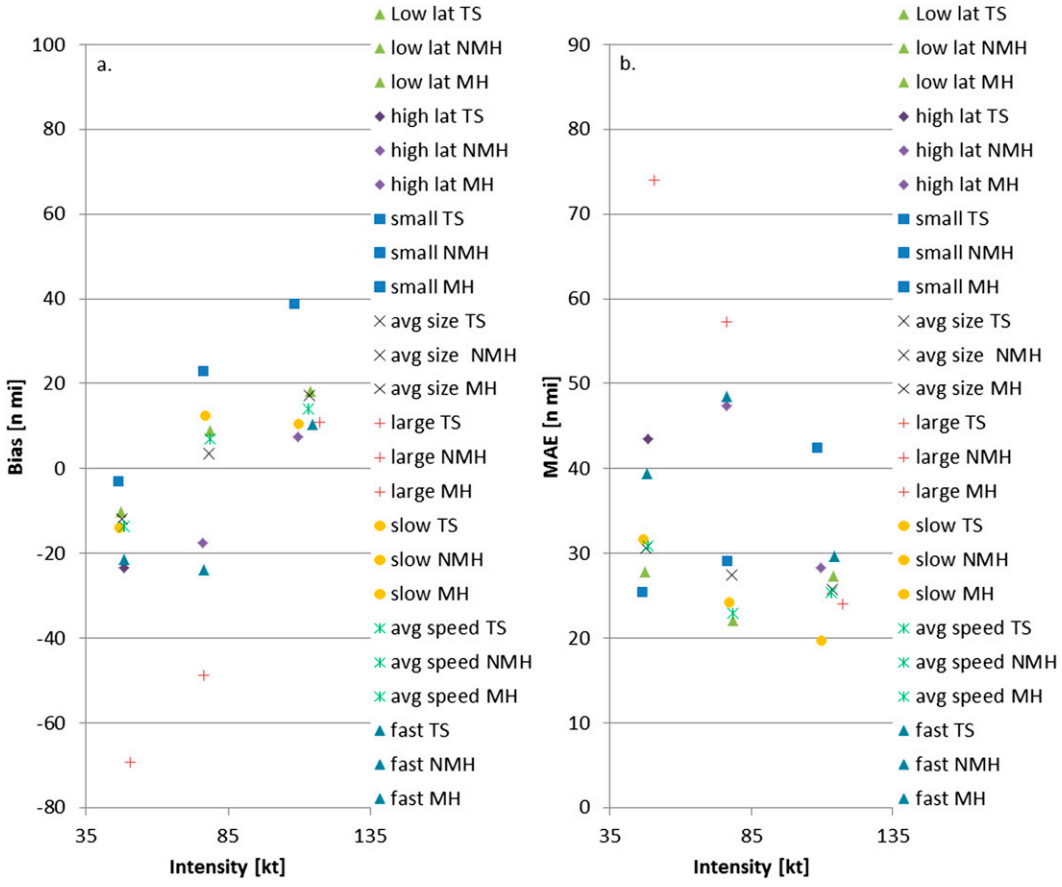

FIG. 3. Size estimate (R5) (a) conditional biases and (b) MAEs associated with the IR-based wind radii algorithm. Stratifications are provided in Table 3 and the number of cases in each composite is provided in Table 4.

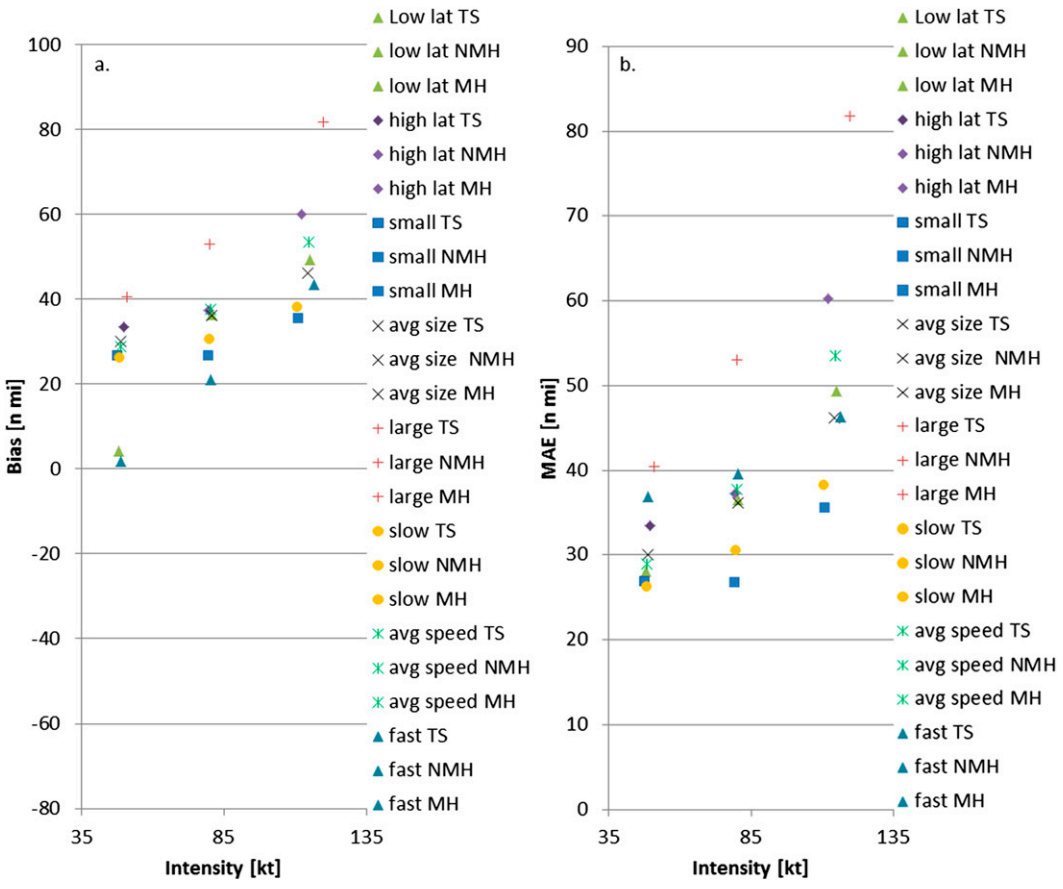

FIG. 4. Size (R5) estimate (a) conditional biases and (b) MAEs associated with the model analysis-based wind radii algorithm. Stratifications are provided in Table 3 and the number of cases in each composite is provided in Table 4.

results in a mean large wind radii bias in the Sandy case. This may be the result of smoothing (our interpolation process or the DA). Nonetheless, mean absolute errors (MAEs) are competitive with other objective wind radii estimation techniques from the Advanced Microwave Sounding Unit (i.e., Demuth et al. 2006), and the combined satellite techniques described in Knaff et al. (2011) that have been reported in the literature.

To better determine strengths and weaknesses of this algorithm, conditional errors and biases are constructed. The conditions are provided in Table 3 and are based on variations of storm location, intensity, translation speed, and size. All of this information is extracted from the advisory information. To ensure an estimated independent size, the radius of the outermost closed isobar is used to create composite errors based on TC size instead of R5. Results of composite MAEs and bias as a function of storm intensity for the nonzero quadrant averages of R34 are now examined.

The nonzero quadrant averages, ''ALL,'' is used as a metric to measure the ability to estimate the extent of 34-kt winds instead of the quadrant average that can be low biased by quadrants where winds do not exceed the 34-kt wind threshold. Figure 3 shows the results based on the IR-based R5 estimates, Fig. 4 shows results from the model analysis-based R5 estimates, and Table 4 provides the number of cases used for the composite error stratifications. The IR-based estimates are made every 3 hours while the analysis-based estimates are made every 6 hours, so the number of IR-based estimates for this dataset is much higher.

The IR-derived results show that the biases associated with this method are a function of intensity (Fig. 3a). Negative biases are shown for tropical storm (TS) cases and positive biases are more prevalent for the major hurricane (MH) cases. Small storms tend to be positively biased and fast moving storms are generally negatively biased. Overall biases are mostly less than 20 n mi. On the other hand, the MAEs associated with the IR-derived wind radii (Fig. 3b) have greater variations as a function of location and motion. The largest MAEs occur for large, high-latitude, and fast-moving

TABLE 4. Number of cases associated with the statistics shown in Figs. 1 and 2.

Condition	Tropical storms (TS)	Nonmajor hurricanes (NMH)	Major hurricanes (MH)
IR-derived wind radii			
Low latitude	4318	1387	947
High latitude	1918	772	148
Small	2783	498	147
Avg size	2849	1232	765
Large	604	429	183
Slow	1466	385	105
Avg speed	3626	1347	781
Fast	1244	437	209
Analysis-derived wind radii			
Low latitude	1853	654	445
High latitude	383	314	63
Small	1112	223	64
Avg size	1190	576	361
Large	148	169	83
Slow	621	165	48
Avg speed	1488	632	364
Fast	404	171	96

TS and nonmajor hurricane (NMH) cases. Other stratifications show quite low MAEs for NMH and TS cases. This method generally performs very well for the MH cases, and with the exception of small MH cases, the MH MAEs are less than 30 n mi.

If model analyses are used to estimate R5 and then wind radii, the biases (Fig. 4a) are again a function of intensity with TS cases having very small biases and MH cases generally having positive biases of 40 n mi. The relatively large biases associated with more intense TCs suggest that the model analyses are providing V500 estimates that are larger than the IR-based algorithm is expecting, especially for MH cases. However, a quick examination of the GFS wind radii from the vortex tracker software (Atlantic and east Pacific 2013–14) provided in the Automated Tropical Cyclone Forecast (ATCF; Sampson and Schrader 2000) databases indicates that the GFS R34 estimates do not show this behavior and have quite small MAE. The R50 and R64 show a tendency to have much larger MAEs, 30% and 100% larger, respectively, and the errors are almost entirely due to large biases. Unlike the results from the IR-derived size estimates, the model analysis-based wind radii show a tendency for biases to become very large for the most intense TCs. Analysis-based wind radii errors and biases are also more directly related to intensity, with the largest MAE occurring for MH cases, particularly for large or high-latitude MH cases. The best performance for the analysis-based wind radii cases are related to small and slow-moving TCs.

TABLE 5. Mean absolute errors (MAE) and bias statistics for 3-hourly IR-derived wind radii estimates for Hurricane Gonzalo (2014). The number of cases for R34, R50, and R64, respectively, is provided by N at the top of each sample. Statistics are shown from individual directional quadrants and from the nonzero average of the individual quadrant wind radii or ALL as explained in the text, which provides an estimate of the overall size errors. Units for these statistics are n mi, where 1 n mi = 1.85 km.

Hurricane Gonzalo results, $N = 65$, $N = 60$, and $N = 56$					
	NE	SE	SW	NW	ALL
R34 MAE	22	36	31	18	24
R34 bias	8	11	26	16	13
R50 MAE	20	25	19	21	21
R50 bias	4	3	18	19	7
R64 MAE	10	18	13	8	12

To provide an example of how the IR-based wind radii would appear to a user, the Hurricane Gonzalo (2014) case is provided here. Gonzalo is a good case to examine because of its tropical origin, its recurving track, and its dense observations and relatively accurate forecasts. Gonzalo also went through two complete eyewall replacement cycles (ERCs), one staring late on 14 October and ending midway through 15 October another late on 16 October that expanded the R_m to 20–25 n mi early on 17 October (Brown 2015)—noting that ERCs are related to wind field expansions (Maclay et al. 2008; Sitkowski et al. 2011). Because 34-kt wind radii are generally better observed than 50- or 64-kt wind radii, we primarily discuss 34-kt wind radii estimates.

Table 5 shows the overall statistics for the Gonzalo case by wind radii and quadrant. The IR-method produced a slight high bias for all wind radii and MAEs that are generally less than the larger independent and dependent samples. The variance explained for the ALL wind radii column, not shown, was 71%, 51%, and 46% for $\overline{\text{R34}}$, $\overline{\text{R50}}$, and $\overline{\text{R64}}$, respectively. Figure 5 shows the time series of wind radii predictions from the IR method (blue) and the best track (black line) that illustrates how the time evolution closely follows the NHC best-track values, though with a bias. Notice that the scheme shows an expansion of the wind field coincident with the final stages of ERC, from 16 to 17 October. Figure 5 also provides wind radii fixes from an AMSU-based method (Demuth et al. 2006) and the vortex tracker output for the GFS model for comparison. These time series show how the IR-based wind radii estimates complement the AMSU and GFS wind radii estimates in real-time TC monitoring.

Continuing the theme of the examination of 34-kt winds associated with Gonzalo, Fig. 6 shows a comparison of IR-based estimates with Advanced

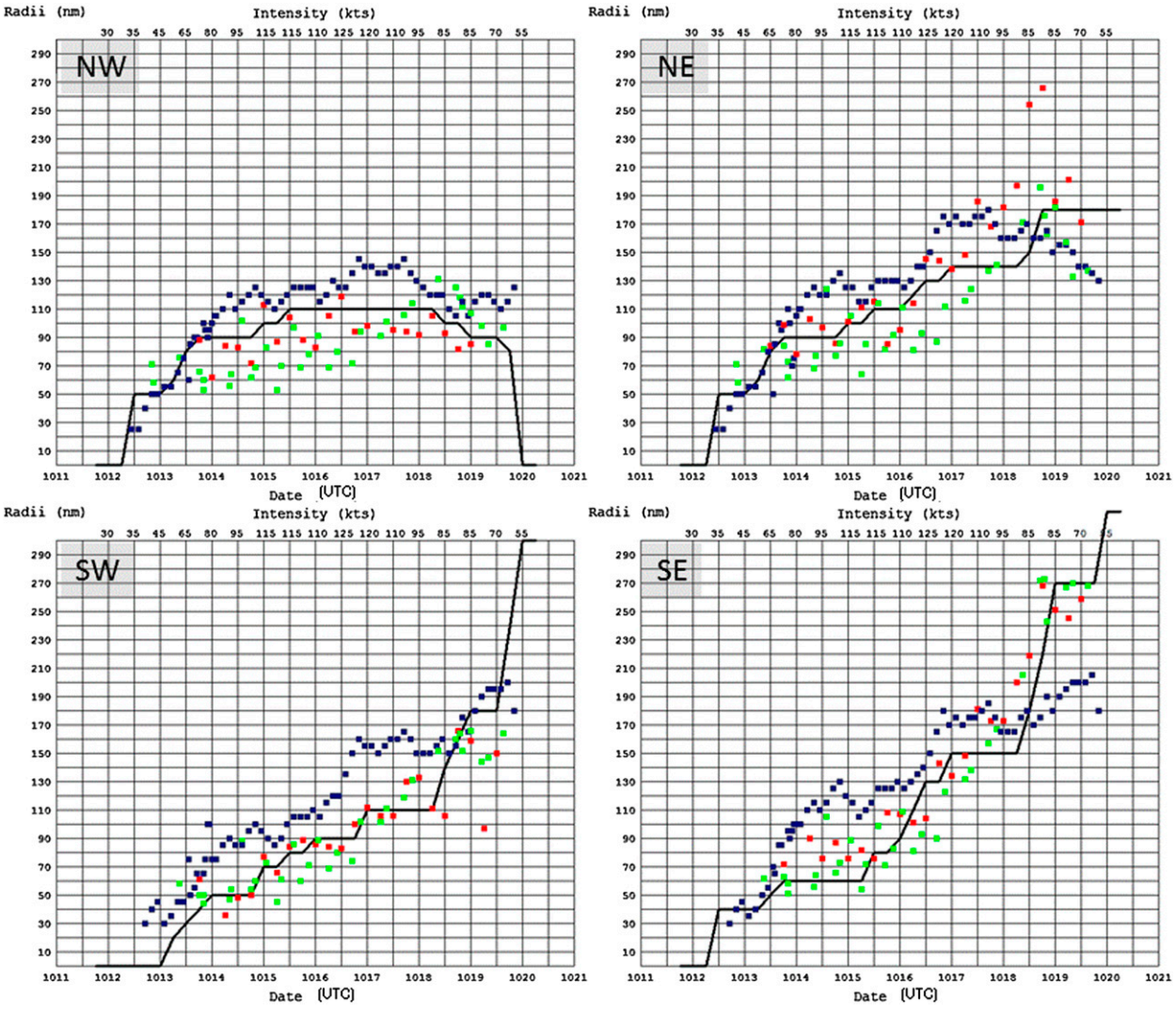

FIG. 5. Time series of IR-based 34-kt wind radii estimates (blue points), AMSU-based 34-kt wind radii estimates (green points), and GFS-based TC tracker 34-kt wind radii (red points) compared to the best track values for Hurricane Gonzalo (2014) (black line). Panels represent the northwest (NW), northeast (NE), southwest (SW), and southeast (SE) storm quadrants. Storm intensities (kt) are listed across the top of each panel.

Scatterometer (ASCAT) wind vectors. The ASCAT retrievals are known to have low biases in TCs and high wind regimes in the tropics (Chou et al. 2013). There were six time periods during the tropical stages of Gonzalo that have sufficient coverage, here we will show four analyses. Figure 6 shows the IR-based wind radii, where 34-, 50-, and 64-kt wind radii are in cyan, maroon, and red, respectively. These are valid essentially at the synoptic time, whereas the scatterometry is the closest available time to that synoptic time. Figure 6 illustrates that the wind asymmetries are likely larger in nature than in the IR-based estimates. Also, there are cases where the IR-based 34-kt wind radii estimates are likely too small (1145 UTC 13 October, northeast quadrant) and too large (1145 UTC 14 October, nearly all quadrants). The IR-method seems to encompass the regions of 30-kt ASCAT surface wind vectors and high biases for this case are evident in the individual times shown here. However, Fig. 6 also illustrates that 34-kt wind radii estimates can be somewhat subjective (constructing wind radii from nearly instantaneous observations) and that the IR-based method compliments other methods to estimate wind radii.

4. Discussion and future directions

A relatively simple method to estimate tropical cyclone wind radii from routinely available information

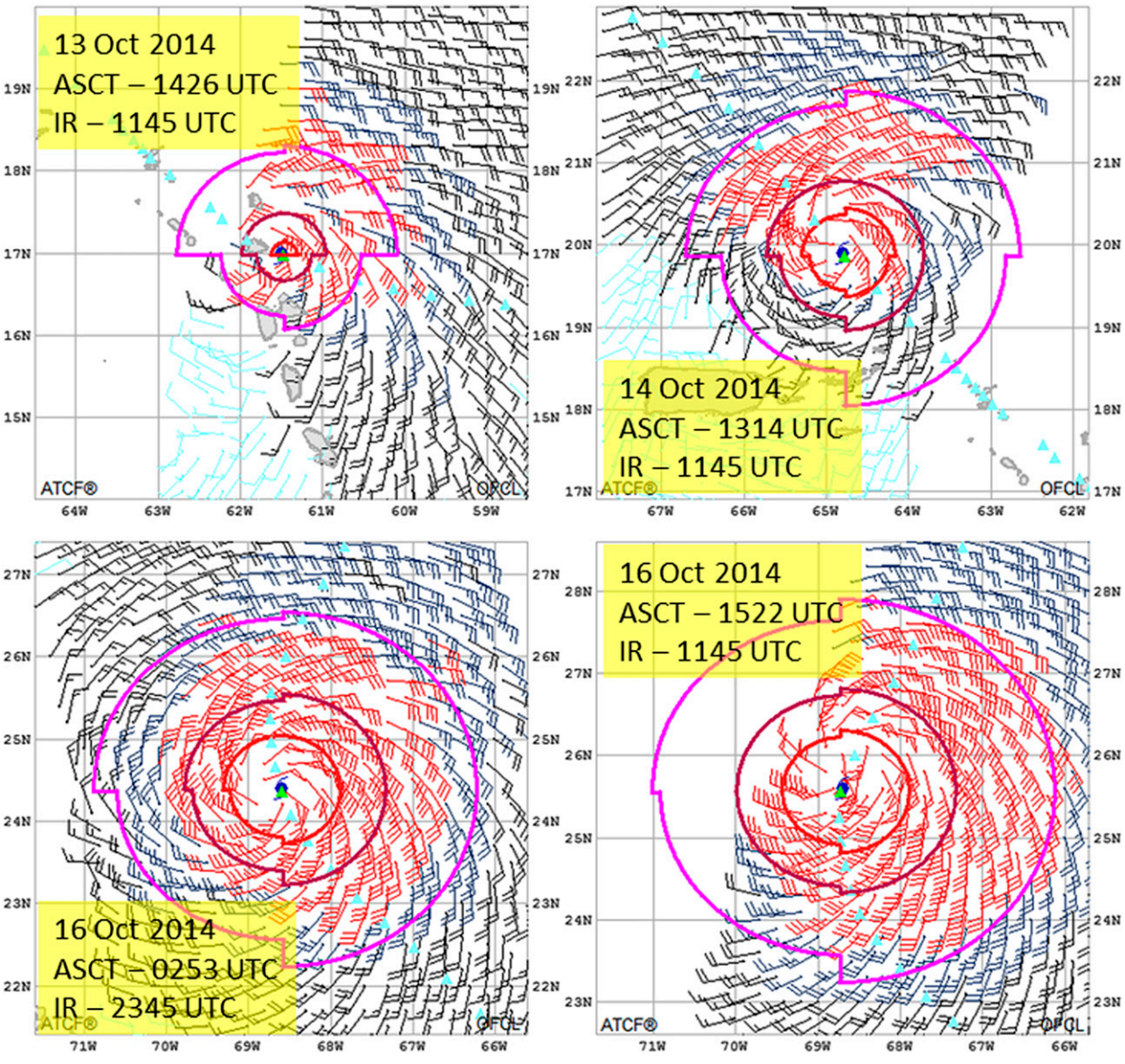

FIG. 6. Advanced Scatterometer (ASCAT) wind vectors are displayed along with IR-based wind radii for Hurricane Gonzalo (2014). ASCAT wind vectors that exceed 30 kt are highlighted in red and estimates of the 34-kt wind radii are shown in magenta. Also included are 50- and 64-kt wind radii as maroon and red lines, respectively. The ASCAT time and IR image time are provided in each panel.

including storm information (location, motion, and intensity) and an estimate of the tangential wind at 500 km (i.e., V500) that is a proxy for TC size (i.e., R5) has been described. The method is constructed from techniques previously published that make assumptions like the simple notion that TCs consist of a symmetric vortex with asymmetries based on storm motion and location. We applied this method using TC size estimates from two different sources: IR satellite imagery and global model analyses. The method using TC size estimates from IR satellite imagery outperformed the method using TC size estimates from global model analyses, possibly because the method was tuned to using the IR satellite imagery. The method provides estimates of wind radii with errors that are comparable to those of other objective methods.

The simplicity of this method makes it adaptable to many applications including providing wind radii estimates for TC intensity fixes such as the operational Dvorak (1984) intensity estimates, providing wind radii to synthetic tracks and historical best tracks, and providing wind radii for global numerical weather prediction models and analyses. Figure 7 illustrates how wind radii could be estimated from the routine Dvorak

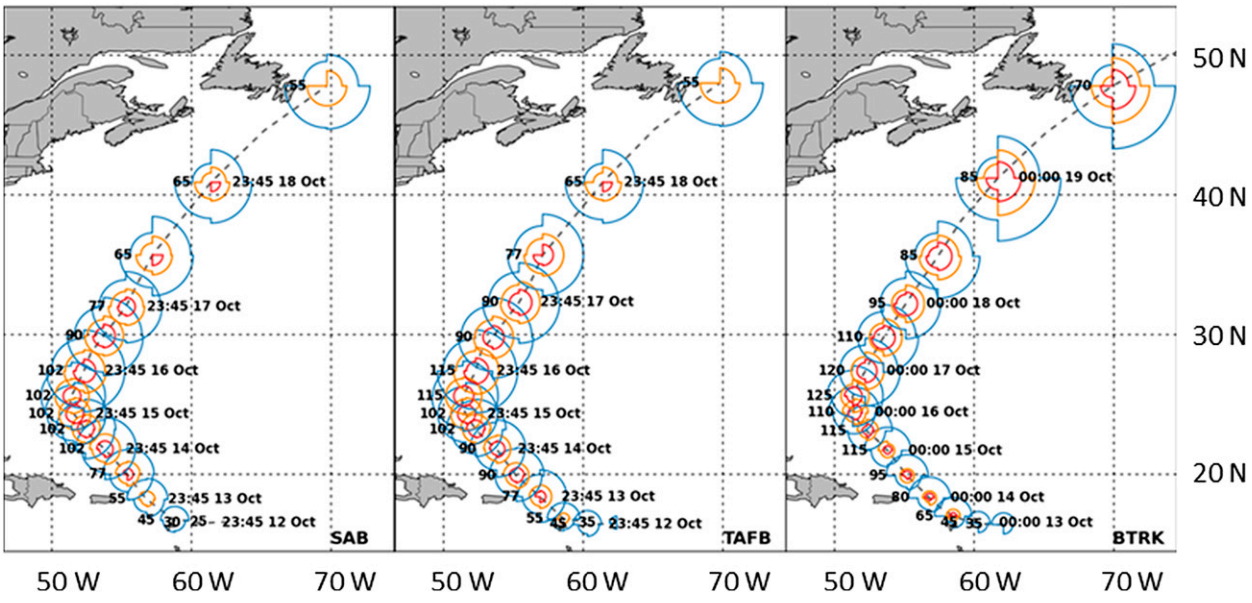

FIG. 7. (left),(middle) Wind radii estimates based on Dvorak intensity and position estimates from SAB and TAFB and (right) radii from the NHC best track for Hurricane Gonzalo (2014). The estimates are shown every 12 h with 34-, 50-, and 64-kt wind radii being displayed in blue, orange, and red, respectively. Intensities of the fixes and best track are provided to the left and dates/times are shown once a day to the right.

intensity estimates from two agencies, the Tropical Analysis and Forecast Branch at the National Hurricane Center (TAFB) and the Satellite Analysis Branch of NOAA/NESDIS (SAB), using Hurricane Gonzalo (2014). The IR-based TC size database used to examine the TC size climatology could be used to provide size distributions and rules (e.g., serial correlation factors, Markov Chains etc.) that could be used in combination with routines that provide synthetic tracks for climatological risk assessments (e.g., Emanuel et al. 2006). Finally, some global numerical modeling systems have shown skill in estimating the 34-kt wind radii (Sampson and Knaff 2015), but still may lack the resolution to accurately estimate 50- and 64-kt wind radii. This method would provide a means to provide wind radii estimates, particularly for R50 and R64; though some simple intensity-based bias correction should be first applied.

Validation of this method shows the reader where the symmetry assumptions break down. In short, this methodology will perform most poorly for TCs that have lower intensities and/or those without a deep convective signal, move fast, are large, or occur at higher latitudes—conditions associated with highly asymmetric TCs and/or those undergoing extratropical transition. Since the error statistics can be estimated from routinely available information, dynamic confidence intervals associated with the estimated wind radii can be estimated using that same information.

There are several avenues for possible future work associated with this algorithm. Possibly the simplest application will be to produce wind radii estimates associated with existing Dvorak-based center and intensity estimates, both subjective (Dvorak 1984) and objective intensity estimation methods (Olander and Velden 2007). To create wind radii for synthetic tracks will take more work, as the TC size distributions and rules needed to constrain the variability of wind radii for synthetic storm tracks still need to be developed from the climatological data discussed in KLM. The potential of assigning wind radii to synthetic tracks would aid in the assessment of wind-forced risks including storm surge—noting that there are methods to estimate central pressure given intensity (V_m), location, motion, wind radii, and TC size as discussed in Courtney and Knaff (2009). If there is interest from the numerical weather prediction community, bias correction and additional testing could result in a more robust statistical method to estimate wind radii based on numerical weather model analyses and forecasts.

Since this methodology seems robust and the satellite record of IR-based TC size is homogeneous over time, it is constructive to investigate 1) the utility of statistical-dynamical prediction of the symmetric IR-based TC size, and 2) the development of historical wind radii for past best tracks. The former is a Joint Hurricane Testbed project and the latter is part of a larger effort to produce

objective best tracks from available intensity, track, and wind radii information at the Naval Research Laboratory, Monterey, California. Finally, this work makes use of a climatological estimate of R_m, but it is clear that while R5 does a good job of estimating 34-kt wind radii variability, the accuracy of the R_m is more important for estimating 50- and 64-kt wind radii. Future work will, therefore, concentrate on producing quality R_m estimates (i.e., better than climatology) from remotely sensed data, especially for weaker TCs and those that do not have an eye structure.

Acknowledgments. This research was supported by NOAA programs including the GOES-R Risk Reduction Program, and the Hurricane Forecast Improvement Program under NOAA Grant NA17RJ1228, and by the Chief of Naval Research through the NRL Base Program, PE 0601153N. In addition, this work made use of techniques developed for the Joint Hurricane Testbed and the display capabilities of ATCF. The methods developed here were also inspired by recent recommendations made at the WMO's Eighth International Workshop on Tropical Cyclones geared toward two goals including: 1) the specification of the entire TC vortex in advisories and forecasts, and 2) the development of homogeneous long-term records of tropical cyclones. We also recognize our work is only possible because of best-tracked wind radii and would like to encourage this practice and the standardization of wind radii types and formats worldwide. Finally, we thank Megan Troutman for her assistance on earlier versions of the manuscript. The views, opinions, and findings contained in this report are those of the authors and should not be construed as an official National Oceanic and Atmospheric Administration or U.S. government position, policy, or decision.

REFERENCES

Bender, M. A., 1997: The effect of relative flow on the asymmetric structure in the interior of hurricanes. *J. Atmos. Sci.*, **54**, 703–724, doi:10.1175/1520-0469(1997)054<0703:TEORFO>2.0.CO;2.

——, I. Ginis, R. Tuleya, B. Thomas, and T. Marchok, 2007: The operational GFDL coupled hurricane–ocean prediction system and summary of its performance. *Mon. Wea. Rev.*, **135**, 3965–3989, doi:10.1175/2007MWR2032.1.

——, M. Morin, T. Marchok, I. Ginis, B. Thomas, and R. E. Tuleya, 2015: Upgrades to the GFDL/GFDN Operational Hurricane Models Planned for 2015. *69th Interdepartmental Hurricane Conf.*, Jacksonville, FL, Office of the Federal Coordinator for Meteorological Services and Supporting Research, S3b-01. [Available online at http://www.ofcm.gov/ihc15/presentations/Session3b/S3b-01-Mbender2015IHC.Tuesday.pptx.]

Brown, D. P., 2015: Hurricane Gonzalo, 12–19 October 2014. National Hurricane Center Tropical Cyclone Rep. AL082014, 30 pp. [Available online at http://www.nhc.noaa.gov/data/tcr/AL082014_Gonzalo.pdf.]

Chan, K. T. F., and J. C. L. Chan, 2013: Angular momentum transports and synoptic flow patterns associated with tropical cyclone size change. *Mon. Wea. Rev.*, **141**, 3985–4007, doi:10.1175/MWR-D-12-00204.1.

——, and ——, 2014: Impacts of initial vortex size and planetary vorticity on tropical cyclone size. *Quart. J. Roy. Meteor. Soc.*, **140**, 2235–2248, doi:10.1002/qj.2292.

Chavas, D. R., and K. A. Emanuel, 2010: A QuikSCAT climatology of tropical cyclone size. *Geophys. Res. Lett.*, **37**, L18816, doi:10.1029/2010GL044558.

Chou, K.-H., C.-C. Wu, and S.-Z. Lin, 2013: Assessment of the ASCAT wind error characteristics by global dropwindsonde observations. *J. Geophys. Res. Atmos.*, **118**, 9011–9021, doi:10.1002/jgrd.50724.

Courtney, J., and J. A. Knaff, 2009: Adapting the Knaff and Zehr wind–pressure relationship for operational use in tropical cyclone warning centres. *Aust. Meteor. Oceanogr. J.*, **58**, 167–179.

DeMaria, M., M. Mainelli, L. K. Shay, J. A. Knaff, and J. Kaplan, 2005: Further improvements in the Statistical Hurricane Intensity Prediction Scheme (SHIPS). *Wea. Forecasting*, **20**, 531–543, doi:10.1175/WAF862.1.

——, J. A. Knaff, R. Knabb, C. Lauer, C. R. Sampson, and R. T. DeMaria, 2009: A new method for estimating tropical cyclone wind speed probabilities. *Wea. Forecasting*, **24**, 1573–1591, doi:10.1175/2009WAF2222286.1.

——, and Coauthors, 2013: Improvements to the operational tropical cyclone wind speed probability model. *Wea. Forecasting*, **28**, 586–602, doi:10.1175/WAF-D-12-00116.1.

Demuth, J., M. DeMaria, J. A. Knaff, and T. H. Vonder Haar, 2004: Validation of an Advanced Microwave Sounder Unit (AMSU) tropical cyclone intensity and size estimation algorithm. *J. Appl. Meteor. Climatol.*, **43**, 282–296, doi:10.1175/1520-0450(2004)043<0282:EOAMSU>2.0.CO;2.

——, ——, and ——, 2006: Improvement of Advanced Microwave Sounding Unit tropical cyclone intensity and size estimation algorithms. *J. Appl. Meteor. Climatol.*, **45**, 1573–1581, doi:10.1175/JAM2429.1.

Developmental Testbed Center, 2015: Gridpoint Statistical Interpolation advanced user's guide version 3.4.0.0. Developmental Testbed Center, 143 pp. [Available online at http://www.dtcenter.org/com-GSI/users/docs/index.php.]

Dvorak, V. F., 1984: Tropical cyclone intensity analysis using satellite data. NOAA Tech. Rep. 11, 45 pp. [Available from NOAA/NESDIS, NOAA/Center for Weather and Climate Prediction, 5830 University Research Court, College Park, MD 20740.]

Emanuel, K., S. Ravela, E. Vivant, and C. Risi, 2006: A statistical deterministic approach to hurricane risk assessment. *Bull. Amer. Meteor. Soc.*, **87**, 299–314, doi:10.1175/BAMS-87-3-299.

Frank, W. M., and E. A. Ritchie, 2001: Effects of vertical wind shear on the intensity and structure of numerically simulated hurricanes. *Mon. Wea. Rev.*, **129**, 2249–2269, doi:10.1175/1520-0493(2001)129<2249:EOVWSO>2.0.CO;2.

Herndon, D., and C. Velden, 2004: Upgrades to the UW-CIMSS AMSU-based tropical cyclone intensity estimation algorithm. *26th Conf. on Hurricanes and Tropical Meteorology*, Miami, FL, Amer. Meteor. Soc., 4D.1. [Available online at https://ams.confex.com/ams/pdfpapers/75933.pdf.]

——, ——, and J. Hawkins, 2012: Update on SATellite-based CONsensus (SATCON) approach to TC intensity estimation. *30th Conf. on Hurricanes and Tropical Meteorology*,

Ponte Vedra Beach, FL, Amer. Meteor. Soc., 7C.2. [Available online at https://ams.confex.com/ams/30Hurricane/webprogram/Paper205129.html.]

Holmlund, K., C. Velden, and M. Rohn, 2001: Enhanced AUTOMATED quality control applied to high-density satellite-derived winds. *Mon. Wea. Rev.*, **129**, 517–529, doi:10.1175/1520-0493(2001)129<0517:EAQCAT>2.0.CO;2.

Jones, W. L., W. L. Grantham, L. C. Schroeder, J. W. Johnson, C. T. Swift, and J. L. Mitchell, 1975: Microwave scattering from the ocean surface. *IEEE Trans. Microwave Theory Tech.*, **23**, 1053–1058, doi:10.1109/TMTT.1975.1128742.

Kalnay, E., 2003: *Atmospheric Modeling, Data Assimilation, and Predictability.* Cambridge University Press, 341 pp.

Knaff, J. A., and R. M. Zehr, 2007: Reexamination of tropical cyclone wind–pressure relationships. *Wea Forecasting*, **22**, 71–88, doi:10.1175/WAF965.1.

——, and B. A. Harper, 2010: KN1: Tropical cyclone surface wind structure and wind-pressure relationships. *Proc. WMO Seventh Int. Workshop on Tropical Cyclones*, La Reunion, France, WMO, 35 pp. [Available online at http://www.wmo.int/pages/prog/arep/wwrp/tmr/otherfileformats/documents/KN1.pdf.]

——, and C. R. Sampson, 2015: After a decade are Atlantic tropical cyclone gale force wind radii forecasts now skillful? *Wea. Forecasting*, **30**, 702–709, doi:10.1175/WAF-D-14-00149.1.

——, ——, M. DeMaria, T. P. Marchok, J. M. Gross, and C. J. McAdie, 2007: Statistical tropical cyclone wind radii prediction using climatology and persistence. *Wea. Forecasting*, **22**, 781–791, doi:10.1175/WAF1026.1.

——, M. DeMaria, D. A. Molenar, C. R. Sampson, and M. G. Seybold, 2011: An automated, objective, multisatellite platform tropical cyclone surface wind analysis. *J. Appl. Meteor. Climatol.*, **50**, 2149–2166, doi:10.1175/2011JAMC2673.1.

——, S. P. Longmore, and D. A. Molenar, 2014: An objective satellite-based tropical cyclone size climatology. *J. Climate*, **27**, 455–476, doi:10.1175/JCLI-D-13-00096.1; Corrigendum, **28**, 8648–8651, doi:10.1175/JCLI-D-15-0610.1.

——, ——, R. T. DeMaria, and D. A. Molenar, 2015: Improved tropical cyclone flight-level wind estimates using routine infrared satellite reconnaissance. *J. Appl. Meteor. Climatol.*, **54**, 463–478, doi:10.1175/JAMC-D-14-0112.1.

Kossin, J. P., J. A. Knaff, H. I. Berger, D. C. Herndon, T. A. Cram, C. S. Velden, R. J. Murnane, and J. D. Hawkins, 2007: Estimating hurricane wind structure in the absence of aircraft reconnaissance. *Wea. Forecasting*, **22**, 89–101, doi:10.1175/WAF985.1.

Lazarus, S. M., S. T. Wilson, M. E. Splitt, and G. A. Zarillo, 2013: Evaluation of a wind-wave system for ensemble tropical cyclone wave forecasting. Part I: Winds. *Wea. Forecasting*, **28**, 297–315, doi:10.1175/WAF-D-12-00054.1.

Lee, C. S., K. K. W. Cheung, W.-T. Fang, and R. L. Elsberry, 2010: Initial maintenance of tropical cyclone size in the western North Pacific. *Mon. Wea. Rev.*, **138**, 3207–3223, doi:10.1175/2010MWR3023.1.

Loridan, T., E. Scherer, M. Dixon, E. Bellone, and S. Khare, 2014: Cyclone wind field asymmetries during extratropical transition in the western North Pacific. *J. Appl. Meteor. Climatol.*, **53**, 421–428, doi:10.1175/JAMC-D-13-0257.1.

Maclay, K. S., M. DeMaria, and T. H. Vonder Haar, 2008: Tropical cyclone inner core kinetic energy evolution. *Mon. Wea. Rev.*, **136**, 4882–4898, doi:10.1175/2008MWR2268.1.

Merrill, R. T., 1984: A comparison of large and small tropical cyclones. *Mon. Wea. Rev.*, **112**, 1408–1418, doi:10.1175/1520-0493(1984)112<1408:ACOLAS>2.0.CO;2.

Mueller, K. J., M. DeMaria, J. A. Knaff, J. P. Kossin, and T. H. Vonder Haar, 2006: Objective estimation of tropical cyclone wind structure from infrared satellite data. *Wea. Forecasting*, **21**, 990–1005, doi:10.1175/WAF955.1.

Musgrave, K. D., R. K. Taft, J. L. Vigh, B. D. McNoldy, and W. H. Schubert, 2012: Time evolution of the intensity and size of tropical cyclones. *J. Adv. Model. Earth Syst.*, **4**, M08001, doi:10.1029/2011MS000104.

Olander, T. L., and C. S. Velden, 2007: The advanced Dvorak technique: Continued development of an objective scheme to estimate tropical cyclone intensity using geostationary infrared satellite imagery. *Wea. Forecasting*, **22**, 287–298, doi:10.1175/WAF975.1.

Ooyama, K., 1969: Numerical simulation of the life cycle of tropical cyclones. *J. Atmos. Sci.*, **26**, 3–40, doi:10.1175/1520-0469(1969)026<0003:NSOTLC>2.0.CO;2.

Probst, P., and G. Franchello, 2012: Global storm surge forecast and inundation modeling. EUR—Scientific and Technical Research Series, EUR 25233 EN-2012, Joint Research Centre, European Commission, 47 pp., doi:10.2788/14951.

Reasor, P. D., M. T. Montgomery, and L. D. Grasso, 2004: A new look at the problem of tropical cyclones in vertical shear flow: Vortex resiliency. *J. Atmos. Sci.*, **61**, 3–22, doi:10.1175/1520-0469(2004)061<0003:ANLATP>2.0.CO;2.

RAMMB/CIRA, 2015: SHIPS: Statistical tropical cyclone intensity forecast technique development. Colorado State University, Fort Collins, CO. [Available online at http://rammb.cira.colostate.edu/research/tropical_cyclones/ships/.]

Rozoff, C. M., D. S. Nolan, J. P. Kossin, F. Zhang, and J. Fang, 2012: The roles of an expanding wind field and inertial stability in tropical cyclone secondary eyewall formation. *J. Atmos. Sci.*, **69**, 2621–2643, doi:10.1175/JAS-D-11-0326.1.

Sampson, C. R., and A. J. Schrader, 2000: The Automated Tropical Cyclone Forecasting System (version 3.2). *Bull. Amer. Meteor. Soc.*, **81**, 1231–1240, doi:10.1175/1520-0477(2000)081<1231:TATCFS>2.3.CO;2.

——, and J. A. Knaff, 2015: A consensus forecast for tropical cyclone gale wind radii. *Wea. Forecasting*, **30**, 1397–1403, doi:10.1175/WAF-D-15-0009.1.

——, P. A. Wittmann, and H. L. Tolman, 2010: Consistent tropical cyclone wind and wave forecasts for the U.S. Navy. *Wea. Forecasting*, **25**, 1293–1306, doi:10.1175/2010WAF2222376.1.

——, and Coauthors, 2012: Objective guidance for use in setting tropical cyclone conditions of readiness. *Wea. Forecasting*, **27**, 1052–1060, doi:10.1175/WAF-D-12-00008.1.

Schubert, W. H., and J. J. Hack, 1982: Inertial stability and tropical cyclone development. *J. Atmos. Sci.*, **39**, 1687–1697, doi:10.1175/1520-0469(1982)039<1687:ISATCD>2.0.CO;2.

Shapiro, L. J., and H. E. Willoughby, 1982: The response of balanced hurricanes to local sources of heat and momentum. *J. Atmos. Sci.*, **39**, 378–394, doi:10.1175/1520-0469(1982)039<0378:TROBHT>2.0.CO;2.

Sitkowski, M., J. P. Kossin, and C. M. Rozoff, 2011: Intensity and structure changes during hurricane eyewall replacement cycles. *Mon. Wea. Rev.*, **139**, 3829–3847, doi:10.1175/MWR-D-11-00034.1.

Smith, R. K., C. W. Schmidt, and M. T. Montgomery, 2011: An investigation of rotational influences on tropical-cyclone size and intensity. *Quart. J. Roy. Meteor. Soc.*, **137**, 1841–1855, doi:10.1002/qj.862.

Tallapragada, V., and Coauthors, 2014: Hurricane Weather Research and Forecasting (HWRF) model: 2014 scientific documentation. Tech. Doc. HWRFv3.6a, Developmental Testbed Center, 105 pp.

[Available online at http://www.dtcenter.org/HurrWRF/users/docs/scientific_documents/HWRFv3.6a_ScientificDoc.pdf.]

Uhlhorn, E. W., B. W. Klotz, T. Vukicevic, P. D. Reasor, and R. F. Rogers, 2014: Observed hurricane wind speed asymmetries and relationships to motion and environmental shear. *Mon. Wea. Rev.*, **142**, 1290–1311, doi:10.1175/MWR-D-13-00249.1.

Velden, C., and Coauthors, 2005: Recent innovations in deriving tropospheric winds from meteorological satellites. *Bull. Amer. Meteor. Soc.*, **86**, 205–223, doi:10.1175/BAMS-86-2-205.

——, and Coauthors, 2006: The Dvorak tropical cyclone intensity estimation technique: A satellite-based method that has endured for over 30 years. *Bull. Amer. Meteor. Soc.*, **87**, 1195–1210, doi:10.1175/BAMS-87-9-1195.

Wilks, D. S., 2006: *Statistical Methods in the Atmospheric Sciences*. 2nd ed. International Geophysics Series, Vol. 91, Academic Press, 627 pp.

Wu, L., W. Tian, Q. Liu, J. Cao, and J. A. Knaff, 2015: Implications of the observed relationship between tropical cyclone size and intensity over the western North Pacific. *J. Climate*, **28**, 9501–9506, doi:10.1175/JCLI-D-15-0628.1.

Xu, J., and Y. Wang, 2010: Sensitivity of the simulated tropical cyclone inner-core size to the initial vortex size. *Mon. Wea. Rev.*, **138**, 4135–4157, doi:10.1175/2010MWR3335.1.

——, and ——, 2015: A statistical analysis on the dependence of tropical cyclone intensification rate on the storm intensity and size in the North Atlantic. *Wea. Forecasting*, **30**, 692–701, doi:10.1175/WAF-D-14-00141.1.